DOI: 10.1021/ma902753y

Macromolecules
ARTICLE

Effect of Hydrophilic Block-A Length Tuning on the Aggregation Behavior of α,ω-Perfluoroalkyl End-Capped ABA Triblock Copolymers in Water

Samuel O. Kyeremateng, Thomas Henze, Karsten Busse, and Jörg Kressler*

Faculty of Chemistry and Physics, Martin Luther University, Von-Danckelmann-Platz 4, D-06120 Halle (Saale), Germany

Received December 13, 2009; Revised Manuscript Received January 26, 2010

ABSTRACT: The tremendous influence of hydrophilic block length tuning on the aggregation behavior of novel water-soluble triphilic (i.e., hydrophilic, lipophilic, and fluorophilic) α,ω-perfluoroalkyl end-capped symmetric ABA triblock copolymers is demonstrated. The hydrophilic A and lipophilic B blocks are comprised of poly(glycerol monomethacrylate) (PGMA) and poly(propylene oxide) (PPO), respectively. The fluorophilic component consists of two "clicked" perfluoroalkyl segments (C_9F_{19}) at the ends of the block copolymers. Two of the different block copolymers synthesized, namely F_9-$PGMA_{24}$-PPO_{27}-$PGMA_{24}$-F_9 (PB1) and F_9-$PGMA_{42}$-PPO_{27}-$PGMA_{42}$-F_9 (PB2), differ only in the degree of polymerization of the hydrophilic PGMA blocks. Their critical micelle concentrations in water are determined from surface tension measurements. The aggregation behavior in aqueous medium studied by ^{19}F NMR spectroscopy reveals that the fluorocarbon component forms part of the micelle corona of PB1, while in PB2 it aggregates to form part of the core. Furthermore, the aggregation behavior studied in aqueous medium by temperature-dependent ^{1}H NMR spectroscopy and DLS measurements showed that PB1 forms only spherical micelles with hydrodynamic radius, R_h, of ~18 nm in solution at all temperatures while PB2 forms mainly aggregate of micelles with R_h of 40 nm at 25 °C. The aggregates disintegrate into compact single "flowerlike" micelles with R_h of ~17 nm at high temperatures. AFM and TEM investigations of the structures formed on solid supports after solvent evaporation also confirm the aggregation behavior of the two block copolymers. The marked difference in the aggregation behavior is a result of the inability of the shorter PGMA blocks of PB1 to loop during micellization and is explained based on random coil statistics.

1. Introduction

In the recent decade the combination of three mutually incompatible fluorophilic, lipophilic, and hydrophilic blocks (i.e., triphilic) in polymer synthesis has generated much interest because of the intriguing structures formed in bulk and in solution.[1−7,9,11−15] The micelle structures formed in aqueous media by these copolymers have mostly a phase-separated core due to the immiscibility between the hydrophobic blocks (fluorophilic and lipophilic) resulting in a multicompartment micelle.[1] Their final morphology depends sensitively on the block copolymer architecture, composition, number of segments, and segment lengths.[1,8] Recently, Lodge et al.[9] demonstrated that micelles with hydrocarbon/fluorocarbon phase-separated cores are able to selectively store hydro- and fluorocarbon chromophores. Such micelles hold very great potentials in the application fields of drug delivery, catalysis, and nanotechnology.[10]

In fact, multicompartment micelles formed by hydrophilic−lipophilic−fluorophilic ABC triblock copolymers of linear[2,11,12] and miktoarm[1] architectures are well documented in the literature. Typically, Li and co-workers have made an in-depth characterization of the diverse morphologies of multicompartment micelles formed by varying the composition of μ-[poly(ethylethylene)][(poly(ethylene oxide)][poly(perfluoropropylene oxide)] miktoarm block copolymers.[1] Multicompartment micelles formed by triblock copolymers with linear and hyperbranched star architectures where the lipophilic and the fluorophilic blocks are separated by the hydrophilic block, i.e., BAC, are also reported.[5,6,13]

However, there are only two studies reporting on the multicompartment micelle structures formed by linear symmetric triphilic pentablock copolymer systems. One of them by Thünemann et al.[3] employs poly(ethylene oxide), poly(γ-benzyl-L-glutamate), and poly(perfluoroether), and the other by He et al.[15] is achieved by end modifying Pluronic 127 with poly(octafluoropentyl methacrylate). In the former, the micelle structure in water is investigated whereas in the latter the effect of the perfluoro block content on the micelle size in water is studied.

This article focuses on the effect of varying the hydrophilic block length on the aggregation behavior of a triphilic α,ω-perfluoroalkyl end-capped ABA triblock copolymer in water. Analogous to a linear symmetric triphilic CABAC pentablock copolymer, the hydrophilic (A), lipophilic (B), and fluorophilic (C) components of our system comprise of poly(glycerol monomethacrylate) (PGMA), poly(propylene oxide) (PPO), and a C_9F_{19} segment, respectively. Whereas PEO-based block copolymers may show LCST behavior at elevated temperatures in water,[15,16] block copolymers with PGMA as hydrophilic block have the advantage of being water-soluble at all temperatures and as such they are suitable candidates for applications where high temperatures maybe a prerequisite.[17] The desired polymer architecture and composition is achieved by employing atom transfer radical polymerization (ATRP) and copper(I)-catalyzed alkyne−azide cycloaddition reaction often referred to as "click" chemistry.[18,19]

*Corresponding author. E-mail: joerg.kressler@chemie.uni-halle.de.

 Published on Web 02/04/2010

Surface tension measurements are employed to determine the critical micelle concentration (cmc) of the block copolymers in water. Futhermore, the influence of the hydrophilic block length on the micelle structures formed in solution is investigated by combining NMR (^{1}H and ^{19}F) spectroscopy and dynamic light scattering (DLS) techniques. Finally, the hydrophilic block length influence is also assessed in terms of structures formed on solid supports by atomic force microscopy (AFM) and transmission electron microscopy (TEM) investigations.

2. Experimental Part

2.1. Polymer Synthesis. The block copolymers were synthesized by atom transfer radical polymerization using copper bromide (CuBr) as catalyst, 2,2′-bipyridine as ligand, and anisole as solvent. Solketal methacrylate (monomer) was polymerized via ATRP at 60 °C using α,ω-dibromo-terminated poly(propylene oxide) (difunctional macroinitiator) as the initiator to give poly(solketal methacrylate-*b*-propylene oxide-*b*-solketal methacrylate), a triblock copolymer of ABA architecture. The ratio of the monomer to initiator was varied depending on the desired degree of polymerization. The polymers were purified by column chromatography followed by precipitation into a cold excess of *n*-hexane. The terminal bromine units of the block copolymers were substituted with N_3 through the azidation reaction with NaN_3 in DMF. Then the terminal N_3 was coupled with nonadecafluoro-1-decyl hex-5-ynoate (perfluorinated segment) through copper(I)-catalyzed 1,3-dipolar cycloaddition reaction to give a α,ω-perfluoroalkyl end-capped ABA triblock. Finally, the block copolymers were rendered triphilic by acid hydrolysis of the water-insoluble poly(solketal methacrylate) blocks to yield water-soluble poly(glycerol monomethacrylate).[17] A detailed experimental procedure for the initiator, perfluorinated segment, and polymer syntheses as well as characterization has been reported previously.[14] The final block copolymers are designated as F_z-$PGMA_y$-PPO_x-$PGMA_y$-F_z, where the subscripts x and y represent the degree of polymerization as determined by ^{1}H NMR while z represents the number of perfluoro carbon atoms in the fluorinated block. Out of the block copolymers synthesized, two of them, F_9-$PGMA_{24}$-PPO_{27}-$PGMA_{24}$-F_9 and F_9-$PGMA_{42}$-PPO_{27}-$PGMA_{42}$-F_9, hereafter referred to as PB1 and PB2, were selected for further characterization. PB1 and PB2 have molar masses of 10 500 and 16 200 g/mol, respectively, as calculated from ^{1}H NMR spectroscopy. Their polydispersities obtained from size exclusion chromatography (SEC) are 1.2 and 1.5, respectively. Scheme 1 illustrates the chemical structures of the two copolymers and the contour lengths of their constituent blocks. Assuming fully extended all-trans conformations between the carbon−carbon bonds, the contour lengths are determined using 2.54 Å for GMA monomer units and for two successive carbon−carbon bonds in the F_9 segments. The PPO contour length calculations are usually based on monomer unit length dimensions between 2.5 and 3.6 Å.[17b,20c] Since the PPO block length is always fixed, we use here as an example the value of 2.5 Å.

2.2. Characterization. *NMR Spectroscopy*. ^{1}H and ^{19}F NMR spectra were recorded from 25 to 60 °C in D_2O and at 25 °C in DMSO-d_6 using Varian magnetic resonance equipment with Gemini 2000 spectrometers operating at 200 MHz. Polymer solutions of concentration 7 g/L were employed. The solutions were prepared by dissolution of appropriate amounts of polymer in solvent followed with slight agitation.

Surface Tension Measurement (*STM*). The surface tension (γ) of the aqueous solutions of the samples at different polymer concentrations was measured by the Wilhelmy plate method using the automated DCAT11 tensiometer (DataPhysics Instruments GmbH, Filderstadt, Germany). Stock solutions of 2.5 g/L were prepared by dissolution of the polymer in bidistilled water, stirred overnight at room temperature, and filtered through 0.45 μm pore-size PTFE before usage. The tensiometer works by automatically injecting predetermined volumes of the stock solution into a thermostated glass vessel containing initially only bistilled water. Following each injection, the surface tension is then measured after 10 min of stirring and a 3 h waiting period. Measurements were carried out at 25 °C by circulating thermostated water accurate to ±0.1 °C.

Scheme 1. Chemical Structure of the PBs Showing the Contour Lengths of the Individual Blocks

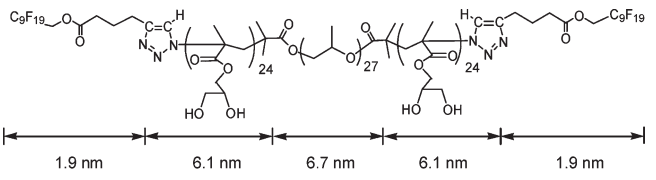

F_9-$PGMA_{24}$-PPO_{27}-$PGMA_{24}$-F_9 (PB1)

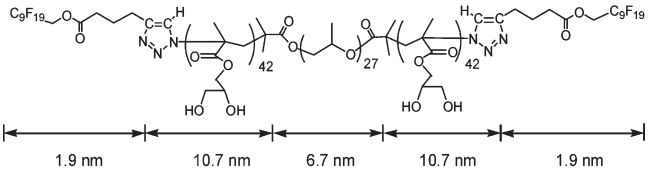

F_9-$PGMA_{42}$-PPO_{27}-$PGMA_{42}$-F_9 (PB2)

Dynamic Light Scattering (*DLS*). DLS measurements of aqueous solutions of the block copolymers were performed using an ALV-NIBS/HPPS automatic goniometer from ALV-Laser (Langen, Germany) in the scattering angle range of 30°−130°. The light source was a neodymium:YAG DPSS-200 laser (λ = 532 nm) with a power output of 200 mW. Intensity time correlation functions were measured with an ALV-5000E multiple-τ digital correlator. The CONTIN algorithm was applied to obtain distribution functions from the obtained autocorrelation function. In case of bimodal distributions, the g^1 autocorrelation function was fitted with two exponential decay functions to obtain an average effective diffusion constant of the two species. The diffusion constant, D_{app}, is related to the reciprocal of the characteristic decay time, Γ, and the scattering vector, q, as $D_{app} = \Gamma/q^2$ [where $q = (4\pi n_0/\lambda)\sin(\theta/2)$, with n_0 = refractive index of the medium, λ = wavelength of the light, and θ = scattering angle]. The corresponding apparent hydrodynamic radii, R_h, were obtained via the Stokes−Einstein equation $R_h = kT/(6\pi\eta D_{app})$, where k is the Boltzmann constant and η is the viscosity of the solvent, water in this case, corrected at the absolute temperature T. Stock solutions of 5.6 g/L were prepared by dissolution of polymers in bidistilled water and stirred overnight. Lower concentrations were prepared by gradual dilution. The solutions were filtered directly into the light scattering cells through a 0.45 μm pore size filter.

Atomic Force Microscopy (*AFM*). AFM images were obtained on a NANOWIZARD I (JPK Instruments, Berlin) operated in tapping mode with silicon cantilevers at a scan rate of 1 Hz. The cantilevers (Arrow, NanoWorld, Neuchâtel) had a resonance frequency of ∼285 kHz and a force constant of ∼42 N/m.

Transmission Electron Microscopy (*TEM*). The TEM images were obtained from a JEOL 100CX microscope, operating at an acceleration voltage of 100 kV. Samples were prepared by drop-coating 0.014 g/L aqueous solutions of polymers on carbon-coated copper grids and allowed to dry under ambient conditions.

3. Results and Discussion

3.1. Surface Tension Measurements. The surface tensions, γ, of aqueous solutions of the block copolymers are measured

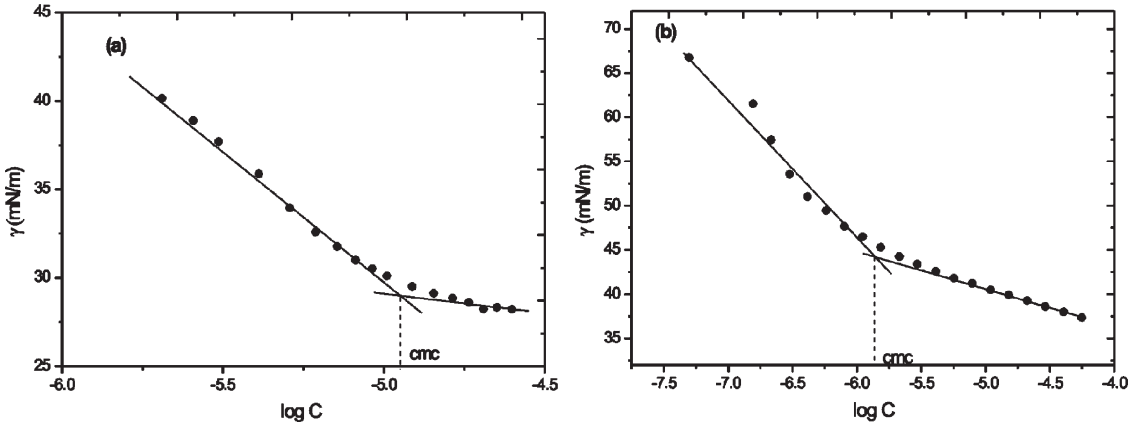

Figure 1. Critical micelle concentration (cmc) determination of (a) PB1 and (b) PB2 from surface tension measurements as a function of concentration at 25 °C.

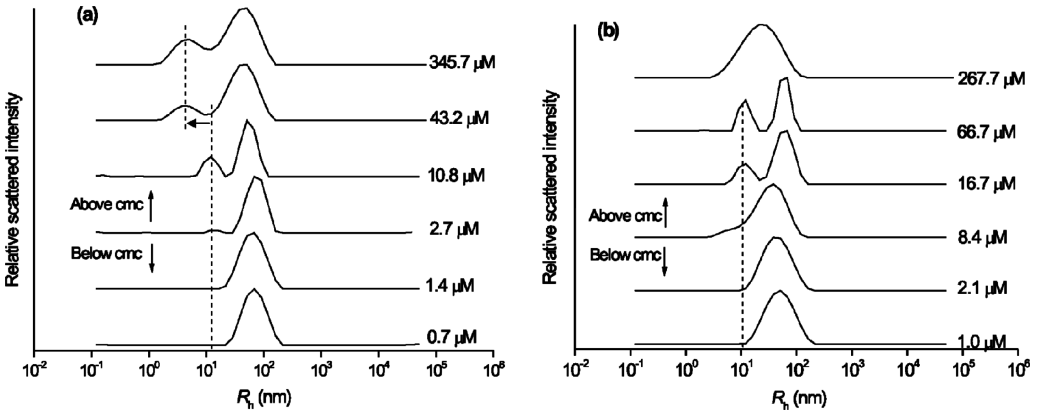

Figure 2. DLS data obtained at $\theta = 90°$ for hydrodynamic radii (R_h) distributions as a function of concentration for aqueous solutions of (a) PB2 and (b) PB1 at 25 °C.

as a function of polymer concentrations at 25 °C. Plotting γ vs polymer concentration (log C) yields the critical micellization concentration (cmc) indicated by intersection of the extrapolation of the two linear regimes where the curves show abrupt change in slope as indicated in Figure 1. The values obtained by this method at 25 °C for PB1 and PB2 are 9.5 and 2.5 μM, respectively.

Unambiguously, the increase of hydrophobicity by shorten of the hydrophilic PGMA block is evidenced by lower values of the surface tension at any given bulk concentration when comparing PB1 with PB2. However, the relatively higher surface activity of PB1 compared to PB2 is not directly translated into a lower cmc value as would be expected from the literature.[20] Moreover, the PB2 curve shows a slight continuous decrease in surface tension values even at concentrations larger than cmc. This significant difference in the surface tension behavior of the two block copolymers with increasing polymer concentration is probably a result of their different micellization mechanism as a function of concentration as discussed in section 3.4. Nevertheless, the inability of PB2 to attain constant γ after cmc is not unusual for triphilic systems containing PPO as the lipophilic component.[15]

3.2. DLS Studies. *Concentration-Dependent Measurements.* DLS studies of aqueous solutions of PGMA homopolymer showed high affinity of the PGMA chains to cluster,[17] similar to other hydroxyl group bearing polymers,[21,22] via formation of intermolecular hydrogen bonds between the pendant hydroxyl groups. A similar phenomenon also occurs with the block copolymers under investigation. At 25 °C and concentrations below cmc, most of the block copolymer chains associate to form unimer-cluster in solution with $R_h \sim 67$ nm as can be seen in Figure 2a for PB2.

On gradual increase of the concentration, some of the block copolymer chains are transferred from the unimer-clusters to form the regular micelles at concentrations around cmc as observed in Figure 2a. In order to confirm that the signals detected really originated from translational diffusion processes, an angular dependent measurement of the decay rates (Γ) between 30° and 130° shown in Figure S1 is performed for the 10.8 μM PB2 aqueous solution. The linear relationships obtained between Γ and the square of the scattering vector, q^2, confirm that the observed peaks are due to diffusive processes.

Further increase in the concentration of the PB2 solution above 10.8 μM leads to an increase in the intensity of the micelle peak until 43.2 μM, when the peak distribution suddenly shift as seen in Figure 2a. The new distribution generated at concentrations of 43.2 μM and above has two species with R_h of 5 and 40 nm. The specie with R_h of 5 nm corresponds to single chains of PB2, and the unsual existence, at least in this particular case, of "free" unimers in solution only at concentrations above cmc is a good proof of the association model of micellization. According to this model, micelles are in equilibrium with single chains above cmc.[23,24] For comparison purpose, the R_h of the single chain can be estimated from the Einstein relation which relates the intrinsic viscosity to polymer volume fraction in solution according to the following

expression:[25]

$$R_h = \left(\frac{3M_n[\eta]}{10\Pi N_A}\right)^{1/3} \quad (1)$$

where M_n, $[\eta]$, and N_A are the molar mass of the polymer, intrinsic viscosity of polymer solution, and Avogadro's number, respectively. The experimental value of $[\eta]$ for PB2 in water is not available. However, the PGMA block makes up 81 wt % of the block copolymer composition; hence, the $[\eta]$ value of 50 mL/g for PGMA in water at 25 °C can be used as a good approximation.[26] The estimated R_h from eq 1 gives 5 nm, which agrees well with the DLS determined unimer size at 25 °C.

It is known that copolymers with BAB architecture upon micellization in a solvent which is selective of the middle block have a tendency to form "flowerlike" micelles and aggregates of micelles through bridging of the middle block at high concentrations.[27,28] Analogously, the block copolymers under investigation can be viewed as having such architecture since the hydrophilic PGMA block is located between two hydrophobic entities (PPO and F_9) and therefore capable of forming such "flowerlike" micelles and aggregate of micelles. It is therefore reasonable to assume that the sudden change in the R_h distribution at concentrations of 43.2 μM and above and the peak distribution with R_h $\sim$ 40 nm generated are most likely due to the formation of such aggregate of micelles. However, it cannot be excluded that this distribution also contains some unimer-cluster which cannot be distinguished from the aggregate of micelles.

Similar to the PB2 solution, PB1 solutions below cmc also contain mostly unimer-clusters with R_h of ~43 nm as shown in Figure 2b. At a concentration close to the cmc, the micelle peak appears as a shoulder on the unimer-cluster peak and continues to increase in intensity with concentration as seen Figure 2b. Increasing the polymer concentration to 268 μM and above, the unimer-cluster peak diminishes, and mostly micelles with R_h of 18.7 nm are found in the solution as depicted in Figure 2b. In Figure S2, the normalized DLS intensity correlation functions, $g^{(1)}(\tau)$, at $\theta = 90°$ and the corresponding relative amplitudes of the micelle and unimer-cluster peaks obtained from the exponential fitting of the correlation functions for the two species are shown for concentrations above cmc. From this figure, the relative amplitude of the micelle species steadily increases from about 0.25 at 16.7 μM to almost 0.5 at 533 μM. It should be emphasized here that, although the unimer-cluster and micelle peaks have comparable amplitudes at this highest concentration, the weight concentration of the unimer-cluster will be small. The ratio of the weight concentrations is given by the relative amplitudes divided by the relative molar masses M_u/M_m.[29] Using the R_h values of the unimer-cluster and micelle peaks, eq 1 can be applied for an approximate estimation of M_m/M_u, which is close to 1/72, and the relative weight concentrations C_u/C_m will thus be about 0.7×10^{-2}. This suggests that at 533 μM the unimer-clusters species in solution constitutes only ~0.7 wt % of the total polymer chains in solution and is of marginal interest. It is also worth mentioning that species with unimer dimensions are not observed in the DLS measurements of PB1 solutions under the given experimental conditions. This lack of unimer or molecular exchange between individual micelles is often referred to as nonergodicity.[30] Furthermore, it seems that the micelles of PB1 do not form aggregates of micelles at high solution concentrations which is contrary to micelles of PB2.

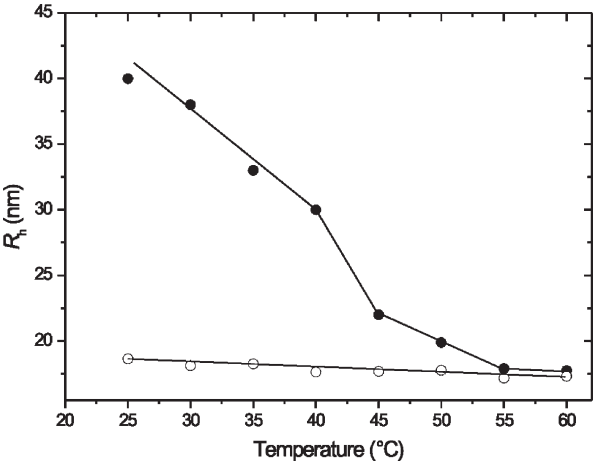

Figure 3. Variation of hydrodynamic radii of aggregates (determined at $\theta = 90°$) as a function of temperature for 5.6 g/L aqueous solutions of PB1 (○) and PB2 (●). The lines through the data are drawn to guide the eye.

Formation of such aggregates of micelles is most likely hindered in PB1 micelles because the contour length of the PGMA block is short and therefore incapable of serving as a bridge between individual micelles as discussed below.

Temperature-Dependent Measurements. Systematic changes in the behavior of the aqueous solutions of the block copolymers with respect to temperature are also investigated in terms of R_h. Figure 3 shows the variation of R_h with temperature for aggregates formed by both block copolymers at a concentration of 5.6 g/L (533 μM for PB1 and 346 μM for PB2), which is above their cmc values at 25 °C.

At 25 °C, PB2 forms mainly aggregate of micelles and unimers in solution with R_h of 40 and 5 nm, respectively, as mentioned above. The R_h value of the aggregate of micelles steadily decreases until 40 °C and then drops to 22 nm at 45 °C. In addition, the single chain peak at 5 nm also starts to disappear at 45 °C as evidenced in Figure S3b. A further decrease in the R_h value of the aggregate of micelles to a typical micelle size of ~17 nm occurs above 55 °C as seen in Figure 3. In summary, high temperature causes the aggregates of micelles to disintegrate into single micelles, and simultaneously all unimers are incorporated into the single micelles.

In contrast, at 25 °C PB1 forms only micelles in solution with R_h of 18.7 nm, which decrease only slightly to 17 nm at 60 °C. The slight decrease in the R_h value of the micelles on increasing temperature can be attributed to slight dehydration of the PPO blocks of the micelle.[31,32] At any given temperature, the R_h values for the PB1 micelles are constant for scattering angle range of 30°−130°, indicating the micelles are spherical in structure.

3.3. NMR Spectroscopy. *^{19}F NMR.* Considering, the particular sequence of the block copolymers architecture, fluorophilic−hydrophilic−lipophilic−hydrophilic−fluorophilic, the hydrophilic blocks are expected to loop to shield the hydrophobic blocks (fluorophilic and lipophilic) from the aqueous environment when micelles are formed. To ascertain whether the F_9 segments are located within the core or corona of the micelle structures formed, ^{19}F NMR measurements were carried at 25 and 50 °C on 7 g/L aqueous solutions of the block copolymers. In Figure 4 the ^{19}F NMR spectra of PB1 solution with the corresponding resonance signals assignment is shown.

At 25 °C high-resolution ^{19}F resonance signals can be observed, an indication that the mobility of the fluorine moieties is not restricted. Thus, the F_9 segments do not

contribute to the formation of the cores of the micelles. Increasing the temperature to 50 °C recorded a better signal resolution. Especially, the signal from the CF_2 unit (labeled 4 in Figure 4) closest to the hydrophilic block becomes very prominent. Additionally, the temperature increase caused an increase in the chemical shift of the resonance signals by ~0.7 ppm. In the literature, such increases in chemical shift and signal resolution have been attributed to increasing mobility of the fluorocarbon moieties.[33,34] Thus, the increase in mobility may be due to breaking of H-bonding between the coronal PGMA chains which consequently leads to increase in mobility the F_9 segments since they are located at the ends of the PGMA blocks.

PB2, on the contrary, did not register any ^{19}F signal when measurements are carried out under identical experimental conditions. Thus, suggesting that the perfluoro F_9 segments in this case are part of the micelle core.

^1H NMR. NMR spectroscopy is a powerful tool for investigating mobility of polymer chains in solution. Figure 5 shows the ^1H NMR spectra of the methyl protons of the PPO (PPO−CH_3) and the PGMA (PGMA−CH_3) blocks of PB1 and PB2 at 25 °C in DMSO-d_6, a nonselective solvent for both blocks as well as the fluorophilic segment.

The peak at 0.76 ppm corresponds to the high content syndiotactic rr triads PGMA methyl protons (rr-PGMA-CH_3), while the peak at 0.93 ppm corresponds to the heterotactic rm triads (rm-PGMA-CH_3) of the same protons.[35] Analysis of the syndiotactic sequence content gives 66%, which is similar to values obtained for poly(methyl methacrylate) (PMMA) prepared by radical polymerization.[36,37] The usual splitting of the PPO methyl protons peak at 1.02 ppm is due to J coupling of the methyl group to the methine group and can be noticed clearly in both spectra.[25] Figure 6 compares the systematic changes in the ^1H NMR spectra with temperature for the PPO−CH_3 and PGMA−CH_3 resonance signals of the two copolymers above cmc in D_2O.

The temperature-dependent residual HDO resonance signal was corrected for each temperature in accordance with earlier studies by Gottlieb et al.[38] In Figure 6a it is clearly evident that the PPO−CH_3 resonance signal intensity of PB1 at 25 °C is highly attenuated relative to the PGMA−CH_3 signals when this spectrum is compared to the counterpart spectrum obtained in DMSO-d_6 at the same temperature

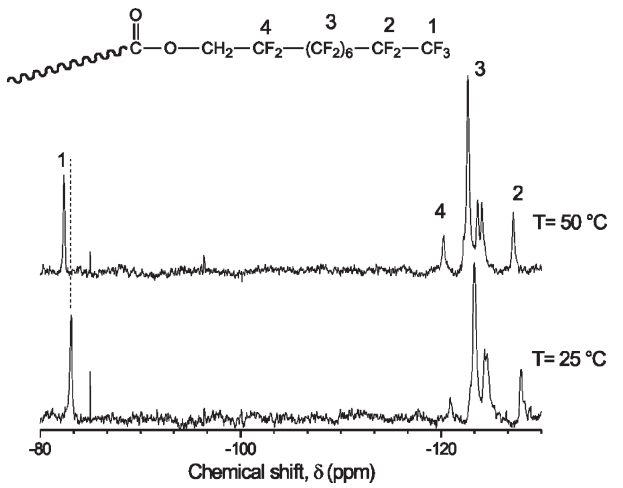

Figure 4. ^{19}F NMR spectra of 7 g/L PB1 in D_2O obtained at 200 MHz for 25 and 50 °C.

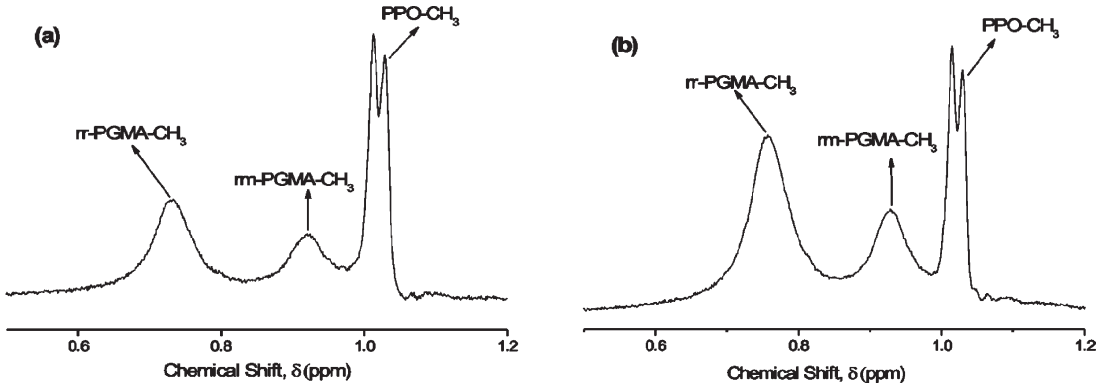

Figure 5. ^1H NMR spectra at 200 MHz of 7 g/L polymer in DMSO-d_6 at 25 °C (a) PB1 and (b) PB2.

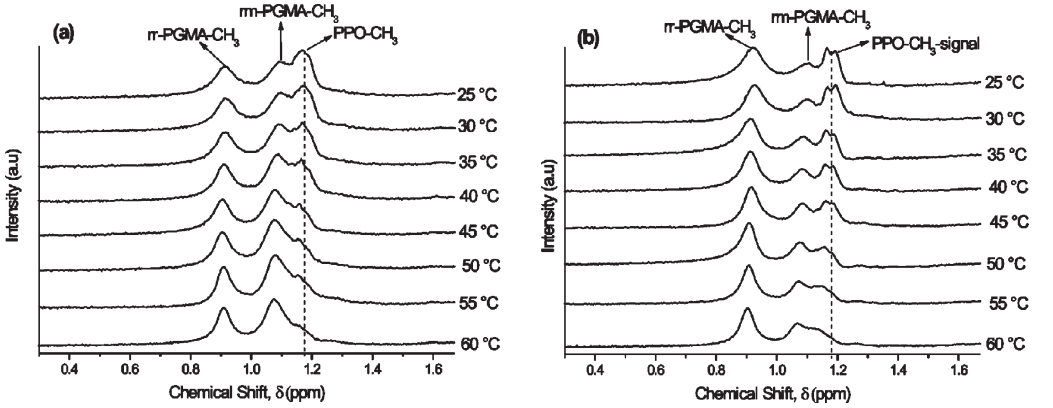

Figure 6. ^1H NMR spectra at 200 MHz of 7 g/L of (a) PB1 and (b) PB2 in D_2O at different temperatures, showing the PGMA−CH_3 and PPO−CH_3 signals. The dashed line represents the position of the PPO methyl protons at 25 °C.

(see Figure 5a). Also, the usual splitting of the PPO−CH_3 resonance signal has completely disappeared and the signal broadened as well. Attenuation, broadening, and disappearance of the splitting of the PPO−CH_3 signal are due to the reduced mobility of the PPO block.[25,27] These significant changes in the PPO−CH_3 resonance signal of PB1 indicate a change in the chemical environment of the methyl protons and signify that the majority of the PPO block is already in the relatively hydrophobic microenvironment of a micelle core.[25,39] This agrees with the DLS results which revealed only single micelles in aqueous solution of PB1 of similar concentration at 25 °C.

Similarly, the PB2 spectrum in D_2O at 25 °C in Figure 6b when compared to the spectrum obtained in DMSO-d_6 (see Figure 5b) also shows attenuation and broadening of the PPO−CH_3 resonance signal relative to the PGMA−CH_3 signals. Although weak, the splitting of the PPO−CH_3 resonance signal can still be noticed. It can therefore be deduced that, at the given concentration and temperature, micellization has already set in, but some block copolymer chains still have their PPO blocks in aqueous environment. The constitution of such polymer chains could originate from micelles which are in their transitional regime as proposed in the micellization mechanism discussed in the next section. With increasing temperature, the PPO resonance signal intensity gradually decreases, and its splitting character completely disappears above 45 °C. This signifies incorporation of the PPO blocks of such chains into the microenvironment of a micelle core.

A clear observation in the ^{1}H NMR spectra of the block copolymers is the shifting of the resonance signal of the PPO−CH_3 upfield with increasing temperature while the PGMA−CH_3 resonance signals remain at relatively the same position. The upfield shift is due to the change in magnetic susceptibility around the PPO−CH_3 protons, owing to the deshielding effect caused by removal of water molecules around the protons.[39] Thus, with increasing temperature the PPO block becomes increasingly dehydrated and hydrophobic.[23,32,40] Almgren et al.[41] as well as Goldmints et al.[32] have established experimentally the existence of significant quantities of water within the PPO core of poloxamers micelles based on small-angle neutron scattering measurements (SANS). Since at 25 °C almost all the PPO block of PB1 exist in the micelle core and considering the fact that PPO of similar molar mass has an LCST at around 15 °C,[42] it implies some water will be trapped within the core. With increasing temperature, further deshielding of the PPO protons and, consequently, upfield shifting occur, but because the core is liquidlike, the signal response of the PPO−CH_3 protons will still be significant. Eventually, the PPO−CH_3 signal completely overlaps with the rm-PGMA−CH_3 signal, resulting in a broader intense single peak at 1.07 ppm at 60 °C (Figure 6a). It can be clearly seen from Figure 6b that this overlap effect is less pronounce in the ^{1}H NMR spectrum of PB2 at 60 °C. This is because the presence of the highly hydrophobic F_9 segments within the micelle cores of PB2 creates a well-dehydrated solidlike environment within the core. Hence, the signal response of the PPO−CH_3 protons in this case is relatively weak. Likewise, at 60 °C there is an overlap of the PPO−CH_3 and the rm-PGMA−CH_3 signals, but the cumulative effect is very weak compared to PB1. In fact, this simple analyses of the temperature-dependent ^{1}H NMR spectra of the two block copolymers conveniently upholds the existence of significant amount of water within micelle cores composed of only PPO as has been proven by SANS measurements.[32,41,43,44] Similar ^{1}H NMR spectra observations regarding partially hydrated PPO cores of PPO−PGMA micelles in aqueous solution at high temperatures have been reported by Save et al.[42]

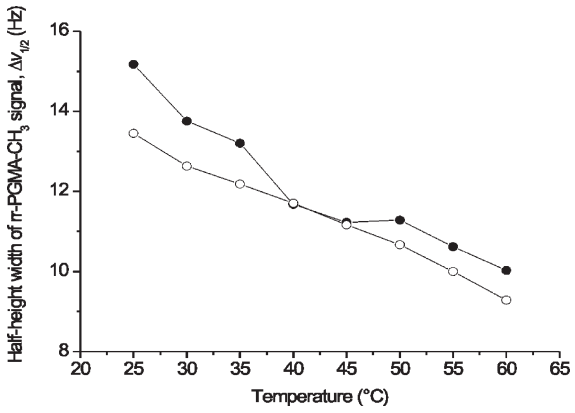

Figure 7. Variation of half-height width of the rr-PGMA−CH_3 resonance signal as a function of temperature for 7 g/L D_2O solutions of PB1 (○) and PB2 (●).

Careful examination of the rr-PGMA−CH_3 resonance peaks at ~0.91 ppm (25 °C) in Figure 6 shows a gradual narrowing of the resonance signals width with increasing temperature for both block copolymers. This suggests that the mobility in the PGMA corona chains increases with temperature for PB1 and PB2 micelles. In ^{1}H NMR spectroscopy measurements, the degree of mobility of a polymer chain in solution is usually assessed by the half-height width, $\Delta\nu_{1/2}$ (the line width at half-height of the highest signal point). Figure 7 shows variation of $\Delta\nu_{1/2}$ in hertz as a function of temperature for the rr-PGMA−CH_3 signals of both block copolymers.

Generally, $\Delta\nu_{1/2}$ decreases linearly with temperature for PB1 solution, which implies the mobility of the PGMA coronal chains increases with temperature as a result of H-bonding breaking between the OH groups of the PGMA blocks. This is in agreement with the earlier results of the ^{19}F NMR spectroscopy measurements of the PB1 solution shown in Figure 4. On the other hand, PB2 shows significantly larger $\Delta\nu_{1/2}$ than PB1 at 25 °C, which decreases rapidly until 40 °C and exhibits a transition between 40 and 50 °C. This indicates that mobility of the PGMA corona chains of PB2 micelles are more restricted than that of PB1 micelles. The higher restriction in mobility of the PGMA blocks in PB2 micelles can be ascribed, in addition to the general H-bonding effect, to the formation of micelle aggregates as observed in the DLS studies. Thus, the closeness of the coronal chains of the component micelles within the aggregate causes further mobility restriction. At 60 °C, when only single micelles exist in solution for both block copolymers as observed by DLS, $\Delta\nu_{1/2}$ for PB1 and PB2 micelles are 9.3 and 10 Hz, respectively. This is an indication that the mobility of the PGMA corona blocks are still more restricted in PB2 micelles than PB1 counterpart, presumably, due to the looping effect of the PB2 PGMA blocks as they do so to sequester the F_9 segments (see ^{19}F NMR discussion).

3.4. Aggregation Mechanism and Loop Formation. Information gathered from DLS and NMR (^{1}H and ^{19}F) spectroscopy at 25 °C indicates that PB2 in aqueous solution above cmc forms micelles and aggregates of micelles with the PPO block and the F_9 segments forming the cores of the micelles. On the basis of this information the following aggregation mechanism is proposed. At concentrations above cmc but less than ~43 μM, unimers are increasingly transferred from the unimer-cluster to form micelles with increasing concentration. Formation of the micelles proceeds by first looping

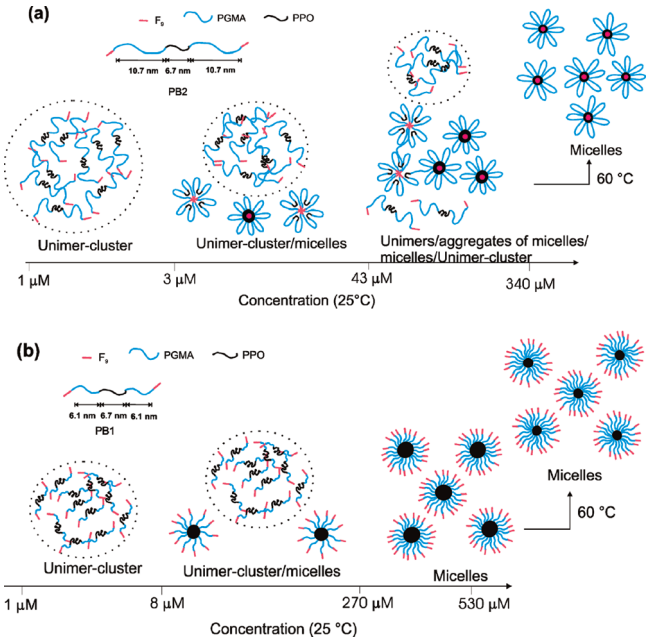

Figure 8. Schematic representation of micelle structures obtained as a result of increasing polymer concentration and temperature of aqueous solutions of (a) PB2 and (b) PB1. The length scales shown below the single chains denote the contour lengths of the respective blocks. In PB1, the short length of the PGMA blocks prevent it from looping; therefore, the F_9 segments cannot be sequestered from the aqueous environment.

of the PGMA blocks to form an aggregated fluorocarbon inner core followed by collapsing of the PPO blocks around the fluorocarbon core to form an outer core. This results in a "flowerlike" micelle structure as illustrated in Figure 8a. Above ~43 μM, connectivity through the PGMA chains takes place between the micelles.

As schematized in Figure 8a, it can be assumed that although micellization is initiated by the F_9 segments, the PPO blocks must completely collapse onto the fluorocarbon core to give the complete inner core−outer core−corona micelle. Further dehydration of the PPO blocks is therefore required to render them hydrophobic enough to collapse onto the highly hydrophobic F_9 core. This further dehydration can be achieved by increasing temperature which leads to obvious dehydration of the PPO block or increase in polymer concentration which leaves less water molecules available for the PPO block hydration. Consequently, it leads to the creation of a solidlike core environment which results in the weak signal response of the PPO block at high temperature as realized in the ^{1}H NMR spectra studies Thus, micelle structures with the PPO blocks not adequately dehydrated to collapsed onto the F_9 core (transitional regime) will still have some mobility in their PPO blocks as observed in the ^{1}H NMR spectra of PB2 solutions at temperatures below 45 °C. It is reasonable to conclude that at high temperature the dehydration and simultaneously contraction of the PPO blocks results in stretching of the interconnecting PGMA chains of the micelle aggregates. However, because the block length of the PGMA chains is not too long, it becomes entropically unfavorable for the interconnectivity to be maintained at high temperature. Eventually, the F_9 segment is expelled, and the PGMA block loops back to incorporate the F_9 segment into the micelle core where the PGMA block is chemically attached. The whole process will lead to the generation of basically only single compact "flowerlike" micelles of PB2 in solution at high temperature, as depicted in Figure 8a.

On the other hand, DLS and NMR (^{1}H and ^{19}F) spectroscopy information obtained leads to the conclusion that, above cmc at 25 °C, PB1 in aqueous solution forms spherical micelles with a core composed of mainly PPO. The PGMA block and the F_9 segments are exposed to the aqueous medium serving as the coronae which stabilize the core. Similar to PB2, unimers of PB1 are increasingly transferred from the unimer-cluster to form micelles with increasing concentration. During the micellization process, the PPO blocks of the copolymer chains simply assemble to form the core of the micelle as schematized in Figure 8b. Thus, the PGMA blocks of PB1 are unable to loop to sequester the F_9 segments into the core.

In studying ABC triblock copolymer of the structure, α-fluorocarbon-ω-hydrocarbon end-capped poly(*N*-acylethylenimine), with degree of polymerization, *N*, for the hydrophilic poly(*N*-acylethylenimine) block being 25, Weberkirch and coworkers[4] realized by ^{19}F NMR spectroscopy measurements in aqueous solution that the micelle formed by this block copolymer is composed of a hydrocarbon core and fluorocarbon end-capped poly(*N*-acylethylenimine) corona. However, with increasing degree of polymerization of the hydrophilic block, specifically $N = 35$, 57, and 75, they found that the micelle structure formed in this case is composed of a core containing both the hydro- and fluorocarbon segments.[5] Thus, short hydrophilic block length prevents looping and that accounts for the absence of the fluorocarbon block in the micelle core. A similar effect of the middle block length on loop formation of ABC triblock copolymer upon micellization has also been observed by other authors.[45]

There are two opposing thermodynamic parameters that determine loop formation: increase of free energy due to looping of the hydrophilic middle block, ΔG_{bend}, and the free energy decrease as a result of the hydrophobic effect (aggregation of hydrophobic segments from the solvent to the micelle core), ΔG_{phobic}. If the magnitude of the former is less than the latter, the loop formed will be stable.[46] In this respect, these parameters are assessed in terms of the transfer of the outer F_9 segment into the micelle cores for the copolymers under investigations. For simplicity, if the enthalpy of mixing between PGMA and water and the repulsive interactions between the F_9 and PPO blocks are ignored, then the free energy of loop formation of the PGMA block can be estimated from[46]

$$\Delta G_{loop} = \Delta G_{bend} + \Delta G_{phobic} \quad (2)$$

On the basis of the end-to-end distribution probability for a Gaussian chain, Alami et al.[29] derived

$$\Delta G_{bend} = -2.6RT + 1.5RT \ln N \quad (3)$$

Furthermore, the free energy gain for transfer of a CH_2 group from water into a micelle core is about $-0.4RT$ per CH_2 group.[29] Since $1CF_2 \approx 1.7CH_2$[50] and there are 4 CH_2 groups linking the F_9 segment to the PGMA block, ΔG_{phobic} for the F_9 segment is therefore estimated as $-7.7RT$. The triazole ring between the PGMA and the F_9 segments is neglected in the estimation because a recent study has proven its hydrophilic contribution as a linker.[51] Substitutions into eqs 3 and 2 yield ΔG_{loop} values of $-5.5RT$ and $-4.7RT$ for PB1 and PB2, respectively. These results derived from the Gaussian statistical model predict that it is thermodynamically feasible for the hydrophilic blocks of both copolymers to loop upon micellization and even more feasible for PB1 to loop than PB2. Based on the model, the results are perfectly reasonable because smaller *N* of the PGMA block of PB1

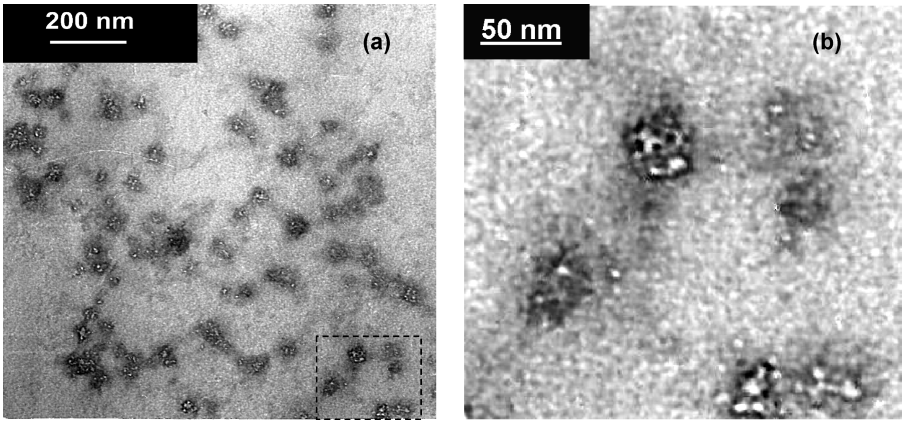

Figure 9. (a) TEM image of PB2 obtained after coating a carbon copper grid with 0.014 g/L aqueous polymer solution and evaporation of water at room temperature. (b) High-magnification image of the area indicated in (a).

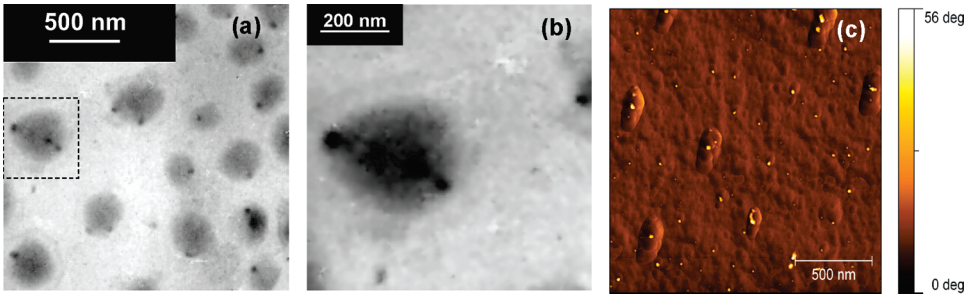

Figure 10. (a) TEM image of PB1 obtained after coating a carbon-coated copper grid with 0.014 g/L aqueous polymer solution and evaporation of water at room temperature. (b) High-magnification image of the aggregate marked with a square in (a). (c) AFM phase image of the same sample used in (a).

implies a smaller end-to-end distance, r ($r \sim N^{1/2}$), hence, higher probability of the two ends of the PGMA block finding each other.[47−49] However, for polymers with low N, as investigated here, the chains are short and therefore semiflexible. The loop formation dynamics of such polymer chains is mainly dominated by needs to overcome the bending energy cost.[52] It then becomes important to take the intrinsic stiffness of the chain into account. The Kuhn length, b, which also closely corresponds to the persistence length, l_p ($b = 2l_p$), characterizes the stiffness of a given polymer chain.[53] Stiffer chains have larger values of b and vice versa. Jun et al.[54] in their analytical results regarding the dynamics of loop formation for a polymer chain with two reactive ends, taking into account intrinsic chain stiffness, concluded that the time required for loop formation, τ_c (closing time), approaches infinity when the length of the polymer chain, $L < 3-4l_p$. Monte Carlo simulation by Chen et al.[55] led to $L < 2.9l_p$, and recent simulation by Toan et al.[56] gave $4l_p$. These results seem to agree and imply that when $L < 3-4l_p$ the bending energy cost is too high for the polymer chain to loop and thus never forms a loop which leads to $\tau_c \rightarrow \infty$.

In this context one can compute the Kuhn segment, $b = lC_\infty$, of the hydrophilic PGMA block using $l = 2.54$ Å as the length of the monomeric unit, and the characteristic ratio, $C_\infty \sim 12$, typical for poly(ethylene glycol methacrylate) in polar solvents is adopted because of its structural similarity to PGMA.[46,57] This gives a value of 3 nm for b and subsequently 1.5 nm as l_p of the PGMA block. Furthermore, computing the contour length, $L = Nl$, of the PGMA blocks give 10.7 and 6.1 nm for PB2 and PB1, respectively, which in turn gives $7l_p$ and $4l_p$, respectively. This means PB1 with its L within the regime where bending energy cost becomes very significant will find it difficult to loop to sequester the F_9 segment into the core. Thus, the analytical and simulation results of literature data discussed above support the micellization behavior of the block copolymers under investigation.

3.5. AFM and TEM Investigations on Polymer Aggregates. The structures formed by coating aqueous solutions of the block copolymers on solid supports are also investigated by TEM and AFM. Figure 9a shows the TEM image obtained by coating 0.014 g/L (0.86 μM) aqueous polymer solution of PB2 on a carbon-coated copper grid and evaporation of the water at room temperature.

Although, the concentration of the solution used is slightly below cmc, it should be realized that as water slowly evaporates from the surface the cmc threshold will be passed and micelles or well-defined aggregates will be formed during this process. The image shows clustering of spherelike aggregates of micelle cores with a diameter size ranging from 20 to 80 nm. AFM height and phase images of PB2, shown in Figure S4, reveal structures with morphology similar to that observed in the TEM image. Figure 9b provides a magnified image of the square marked in Figure 9a. One of such a well-defined aggregate with a diameter of about 50 nm is shown in the upper part of this image. This aggregate shows segregated dark domains of an average diameter of 5.4 nm. Aggregated fluorocarbons domains are known to create a dark contrast in TEM images because of their high electron density.[58,59] The dark domains in Figure 9b can therefore be attributed to the aggregated F_9 segments forming an inner core, and the white surrounding outer core matrix is obviously caused by the PPO. By careful inspection of the aggregate, one can notice the noncontinuity in the white PPO outer cores as a result of the barriers created by the gray PGMA contrast. This suggests that the aggregate, indeed, consists of

individual micelles which are composed of distinct F_9 inner core, PPO outer core, and PGMA corona as depicted schematically in Figure 8a. Obviously, the segregation is the result of the immiscibility between the perfluoro segments and the PPO blocks.[60,61] It results in the formation of a compartmentalized core.[3] The gray contrast emanating from the hydrophilic PGMA blocks can be noticed on the surface and the peripherals of the aggregates.

Contrary to PB2, the TEM image of PB1 in Figure 10a shows large spherical gray aggregates of a diameter between 80 and 400 nm with isolated dark spots. The sample was prepared under conditions identical to PB2.

A close look at one of the aggregates marked with a square in Figure 10a and enlarged in Figure 10b shows that the diameter of the dark spots is ~35−40 nm. As indicated above, the dark spots in the TEM image can be attributed to aggregated perfluoro F_9 segments of PB1. An AFM phase imaging carried out on the polymer-coated grid used for the TEM is shown in Figure 10c. Although within this scan area the aggregates are embedded in a polymer film with an irregular shape, the isolated spots can still be noticed as white spots on the aggregates. It is known that phase contrast in AFM imaging is due to differences in viscoelastic properties of the material.[62] Thus, the hard aggregated perfluoro domains of PB1 appear as the white spots in the AFM phase image. At the moment, the exact mechanism behind formation of such large aggregates is not clear. However, it seems that the initially formed PB1 micelles in an attempt to reduce the interfacial energy between their fluorophilic surfaces and the hydrophobic support cluster to form such aggregates. The nonergodic character of PB1 micelles in solution as observed in the DLS studies may also contribute as well since such behavior is known to lead also to the formation of large compound micelles.[29,62]

4. Conclusions

Water-soluble triphilic α,ω-perfluoroalkyl end-capped ABA triblock copolymers have been synthesized by ATRP and "click" chemistry and characterized. Two of the block copolymers F_9-$PGMA_{24}$-PPO_{27}-$PGMA_{24}$-F_9 (PB1) and F_9-$PGMA_{42}$-PPO_{27}-$PGMA_{42}$-F_9 (PB2) were selected for further studies because of the marked difference in their behavior in aqueous solution. In aqueous solution, above cmc, PB2 formed micelles and aggregates of micelles which disintegrated into single micelles at high temperature. For the PB2 micelles, the PGMA blocks formed the corona while the PPO block and the F_9 segments formed the core. The immiscibility between the F_9 segments and the PPO blocks within the core resulted in a compartmentalized core where they formed the inner and the outer cores, respectively. In contrast, single spherical micelles with PPO core and F_9-terminated PGMA coronal chains were formed by PB1 in aqueous solution above cmc. Evidence of the perfluoro F_9 segments forming part of the coronal chains was obtained from ^{19}F NMR spectroscopy. The effect of the presence or the absence of the F_9 segments within the micelle cores of the two block copolymers was reflected in the temperature-dependent ^1H NMR behavior of their PPO blocks. The lack of the F_9 segments within the core of PB1 micelles is due to the inability of their short rigid PGMA blocks to loop. This observation is in agreement with theoretical prediction of loop formation by semiflexible polymer chain and accounts for the strong difference in aggregation behavior of these two structurally similar block copolymers. While there have been many reports on multicompartment micelles formed by triblock copolymers, reports on such perfluoroalkyl end-capped symmetric ABA triblock copolymers are rare. Also, the effect of hydrophilic block length on loop formation in "flowerlike" micelles has been rarely reported. These combinations make the results of this study unique and interesting.

Acknowledgment. We thank the Deutsche Forschungsgemeinschaft (DFG), FOR 1145 for the financial support. Special thanks to Robert Sachsenhofer (Chemistry Department) and Thomas Thurn-Albrecht (Physics Department) of Martin Luther University for their assistance with the TEM and AFM images, respectively.

Supporting Information Available: Relaxation rate (Γ) as a function of the square of the magnitude of the scattering vector (q^2) at 25 °C for 10.8 μM aqueous solutions of PB2, DLS intensity correlation functions and the corresponding relative amplitude of micelle and unimer-cluster peaks for PB1 aqueous solutions, DLS data obtained for hydrodynamic radii (R_h) distributions as a function of temperature for aqueous solutions of PB1 and PB2, and AFM image of PB2 aggregates formed on a solid support. This material is available free of charge via Internet at http://pubs.acs.org.

References and Notes

(1) Li, Z.; Hillmyer, M. A.; Lodge, T. P. *Langmuir* **2006**, *22*, 9409–9417.
(2) Zhou, Z.; Li, Z.; Ren, Y.; Hillmyer, M. A.; Lodge, T. P. *J. Am. Chem. Soc.* **2003**, *125*, 10182–10183.
(3) Thünemann, A. F.; Kubowicz, S.; Berlepsch, H.v.; Möhwald, H. *Langmuir* **2006**, *22*, 2506–2510.
(4) Weberkirch, R.; Preuschen, J.; Spiess, H. W.; Nuyken, O. *Macromol. Chem. Phys.* **2000**, *201*, 995–1007.
(5) Kubowicz, S.; Thünemann, A. F.; Weberskirch, R.; Möhwald, H. *Langmuir* **2005**, *21*, 7214–7219.
(6) Mao, J.; Ni, P.; Mai, Y.; Yan, D. *Langmuir* **2007**, *23*, 5127–5134.
(7) Lodge, T. P.; Hillmyer, M. A.; Zhou, Z. *Macromolecules* **2004**, *37*, 6680–6682.
(8) (a) Zhao, Y.; Liu, Y.-T.; Lu, Z.-Y.; Sun, C.-C. *Polymer* **2008**, *49*, 4899–4909. (b) Zhang, H.; Ni, P.; He, J.; Liu, C. *Langmuir* **2008**, *24*, 4647–4654.
(9) Lodge, T. P.; Rasdal, A.; Li, Z.; Hillmyer, M. A. *J. Am. Chem. Soc.* **2005**, *127*, 17608–17609.
(10) Ott, C.; Hoogenboom, R.; Hoeppener, S.; Wouters, D.; Gohy, J.-F.; Schubert, U. S. *Soft Matter* **2009**, *5*, 84–91.
(11) Kubowicz, S.; Baussard, J.-F.; Lutz, J.-F.; Thünemann, A. F.; Berlesch, H.; Laschewsky, A. *Angew. Chem., Int. Ed.* **2005**, *44*, 5262–5265.
(12) Skrabania, K.; Laschewsky, A.; Berlepsch, H.v.; Böttcher, C. *Langmuir* **2009**, *25*, 7594–7601.
(13) Berlepsch, H.v.; Böttcher, C.; Skrabania, K.; Laschewsky, A. *Chem. Commun.* **2009**, 2290–2292.
(14) Kyerematen, S. O.; Amado, E.; Blume, A.; Kressler, J. *Macromol. Rapid Commun.* **2008**, *29*, 1140–1146.
(15) He, J.; Ni, P.; Liu, C. *J. Polym. Sci., Part A: Polym. Chem.* **2008**, *46*, 3029–30431.
(16) Bruijn, V. G.; Broeke, L. J. P.; Leermakers, F. A. M.; Keurenttjes, J. T. F. *Langmuir* **2002**, *18*, 10467–10474.
(17) (a) Kyerematen, S. O.; Amado, E.; Kressler, J. *Eur. Polym. J.* **2007**, *43*, 3380–3391. (b) Amado, E.; Augsten, C.; Mäder, K.; Blume, A.; Kressler, J. *Macromolecules* **2006**, *39*, 9486–9496.
(18) Tsarevsky, N. V.; Summerlin, B. S.; Matyjaszewki, K. *Macromolecules* **2005**, *38*, 3558–3561.
(19) Opsteen, J. A.; Van Hest, J. C. M. *J. Polym. Sci., Part A: Polym. Chem.* **2007**, *45*, 2913–2924.
(20) (a) Alexandridis, P.; Athanassiou, V.; Fukuda, S.; Hatton, T. A. *Langmuir* **1994**, *10*, 2604–2612. (b) Alexandridis, P.; Holzwarth, J. F.; Hatton, T. A. *Macromolecules* **1994**, *27*, 2414–2425. (c) Wanka, G.; Hoffmann, H.; Ulbricht, W. *Macromolecules* **1994**, *27*, 4145–4159.
(21) Fang, L.; Brown, W. *Macromolecules* **1990**, *23*, 3284–3290.
(22) Madsen, J.; Armes, S. P. *Biomacromolecules* **2009**, *10*, 1875–1887.
(23) Hvidt, S.; Trandum, C.; Batsberg, W. *J. Colloid Interface Sci.* **2002**, *250*, 243–250.
(24) Zhu, Z.; Xu, J.; Zhou, Y.; Jiang, X.; Armes, S. P.; Liu, S. *Macromolecules* **2007**, *40*, 6393–6400.
(25) Cau, F.; Lacelle, S. *Macromolecules* **1996**, *29*, 170–178.

(26) Pezron, E.; Leibler, L.; Ricard, A.; Lafuma, F.; Audebert, R. *Macromolecules* **1989**, *22*, 1169–1174.
(27) Riess, G. *Prog. Polym. Sci.* **2003**, *28*, 1107–1170.
(28) Balsara, N. P.; Tirrell, M.; Lodge, T. P. *Macromolecules* **1991**, *24*, 1975–1986.
(29) Alami, E.; Almgren, M.; Brown, W. *Macromolecules* **1996**, *29*, 2229–2243.
(30) Won, Y.-Y.; Bates, F. S. In *Giant Micelles, Properties and Applications*; Zana, R., Kaler, E. W., Eds.; CRC Press: Boca Raton, FL, 2007; pp 418−451.
(31) Kositza, M. J.; Bohne, C.; Alexandridis, P.; Hatton, T. A.; Holzwarth, J. F. *Macromolecules* **1999**, *32*, 5539–5551.
(32) Goldmints, I.; Yu, G.-E.; Booth, C.; Smith, K. A.; Hatton, T. A. *Langmuir* **1999**, *15*, 1651–1656.
(33) Preuschen, J.; Menchen, S.; Winnik, M. A.; Heuer, A.; Spiess, H. W. *Macromolecules* **1999**, *32*, 2690–2695.
(34) Zhang, H.; Pan, J.; Hogen-Esch, T. E. *Macromolecules* **1998**, *31*, 2815–2821.
(35) Carriere, P.; Grohens, Y.; Spevacek, J.; Schultz, J. *Langmuir* **2000**, *16*, 5051–5053.
(36) Chen, G.; Zhu, X.; Cheng, Z.; Lu, J.; Chen, J. *Polym. Int.* **2004**, *53*, 357–363.
(37) Wang, J.-S.; Matyjaszewski, K. *Macromolecules* **1995**, *28*, 7901–7910.
(38) Gottlieb, H. E.; Kotlyar, V.; Nudelman, A. *J. Org. Chem.* **1997**, *62*, 7512–7515.
(39) Ma, J.-H.; Guo, C.; Tang, Y.-L.; Liu, H.-Z. *Langmuir* **2007**, *23*, 9596–9605.
(40) Guo, C.; Liu, H. Z.; Chen, J. Y. *Colloid Polym. Sci.* **1999**, *277*, 376–381.
(41) Almgren, M.; Brown, W.; Hvidt, S. *Colloid Polym. Sci.* **1995**, *273*, 2–15.
(42) Save, M.; Weaver, J. V. M.; Armes, S. P.; McKenna, P. *Macromolecules* **2002**, *35*, 1152–1159.
(43) Yang, L.; Alexandridis, P.; Steyler, D. C.; Kositza, M. J.; Holzwarth, J. F. *Langmuir* **2000**, *16*, 8555–8561.
(44) Pedersen, J. S.; Gerstenberg, M. C. *Colloids Surf., A* **2003**, *213*, 175–187.
(45) Cai, Y.; Armes, S. P. *Macromolecules* **2004**, *37*, 7116–7122.
(46) Maiti, S.; Chatterji, P. R. *J. Phys. Chem. B* **2000**, *104*, 10253–10257.
(47) Sperling, L. H. *Introduction to Physical Polymer Science*, 3rd ed.; John Wiley & Sons: New York, 2001.
(48) ten Brinke, G.; Hadziioannou, G. *Macromolecules* **1987**, *20*, 486–489.
(49) Raspaud, E.; Lairez, D.; Adam, M.; Carton, J.-P. *Macromolecules* **1994**, *27*, 2956–2964.
(50) Hussain, H.; Busse, K.; Kressler, J. *Macromol. Chem. Phys.* **2003**, *204*, 936–946.
(51) Reuter, S.; Busse, K.; Radics, U.; Niclas, H.-J.; Kressler, J. *J. Colloid Interface Sci.* **2009**, *340*, 276–284.
(52) Santo, K. P.; Sebastian, K. L. *Phys. Rev. E: Stat., Nonlinear, Soft Matter Phys.* **2006**, *73*, 0319231–03192315.
(53) Strobl, G. *The Physics of Polymers*, 2nd ed.; Springer-Verlag: Berlin, 1996.
(54) Jun, S.; Bechhoefer, J.; Ha, B.-Y. *Europhys. Lett.* **2003**, *64*, 420–426.
(55) Chen, J. Z. Y.; Tsao, H.-K.; Sheng, Y.-J. *Europhys. Lett.* **2004**, *65*, 407–413.
(56) Toan, N. M.; Morrison, G.; Hyeon, C.; Thirumalai, D. *J. Phys. Chem. B* **2008**, *112*, 6094–6106.
(57) Bohdanecky, M.; Tuzar, Z. *Collect. Czech. Chem. Commun.* **1969**, *34*, 3318–3324.
(58) Kubowicz, S.; Baussard, J.-F.; Lutz, J.-F.; Thünemann, A. F.; Berlesch, H.; Laschewsky, A. *Angew. Chem., Int. Ed.* **2005**, *44*, 5262–5265.
(59) Busse, K.; Kressler, J.; Eck, D.; Höring, S. *Macromolecules* **2002**, *35*, 178–184.
(60) Zhou, Z.; Li, Z.; Ren, Y.; Hillmyer, M. A.; Lodge, T. P. *J. Am. Chem. Soc.* **2003**, *125*, 10182–10183.
(61) Li., Z.; Kesselman, E.; Talmon, Y.; Hillmyer, M. A.; Lodge, T. P. *Science* **2004**, *306*, 98–101.
(62) Njikang, G.; Han, D.; Wang, J.; Liu, W. *Macromolecules* **2008**, *41*, 9727–9735.